J Mater Sci (2006) 41:7555–7561
DOI 10.1007/s10853-006-0840-y

Transmission electron microscopy observations on the microstructure of naturally aged Al–Mg–Si alloy AA6022 processed with an electric field

H. Conrad · S. Ramachandran · K. Jung · J. Narayan

Received: 10 October 2005 / Accepted: 3 November 2005 / Published online: 26 September 2006

Abstract The influence of an electric field applied during the solution heat treatment and during a short subsequent initial natural aging of AA6022 on the nature of the precipitates which occurred after natural aging for a long time (2–3 years) was determined employing transmission electron microscopy and selected area electron diffraction. The precipitates were spherical in shape ranging from 2 nm to 40 nm in diameter d_p with an average of 7.9 nm. Their average size was larger than that (4.9 nm) in a specimen processed without field and their size distribution had a greater number of precipitates with d_p>~3 nm. Moreover, their crystal structure differed from that in specimens processed without a field. The increase in yield stress which occurred with the electric field treatments is attributed to an increase in the interaction force between the precipitates and dislocations, which resulted from the larger size and different crystal structure of the precipitates by the field.

Introduction

In prior work [1, 2] it was found that the application of an electric field during the solution heat treatment (SHT) of the Al–Mg–Si alloys AA6022 and AA6111 increased the solubility of the pertinent solutes and in turn the tensile properties in the naturally aged T4 temper. In a separate study [3] it was found that the application of an electric field for a short time during initial natural aging (INA) immediately following the quench further enhanced the tensile properties. The objective of the present research was to determine the nature of clusters or precipitates, which occurred upon long-time natural aging of AA6022 following the application of an electric field during both SHT and INA. Of special interest is a comparison of the microstructure of specimens processed with a field compared to that without a field, but naturally-aged for the same period (2–3 years).

Based on studies employing differential scanning calorimetry (DSC) from R.T. to 550 °C along with atom probe field ion microscopy (APFIM) and transmission electron microscopy (TEM), Edwards et al. [4] reported the precipitation sequence given in Fig. 1 for the Al–Mg–Si alloy AA6061 processed without an electric field. The Mg:Si atom ratios in the Mg/Si clusters, the small precipitates of unknown structure and the β'' and B′ precipitates were all approximately 1:1. Additional information on the characteristics of the various clusters and precipitates in Al–Mg–Si alloys is given in Table 1.

Summarized in Table 2 are studies on the clusters or precipitates, which occur during *natural aging* of Al–Mg–Si alloys. Dotty contrasts were observed with regular transmission electron microscopy (TEM) in specimens naturally aged up to 88 days, but there was no distinct evidence of prespitates. With high resolution transmission electron microscopy (HRTEM), very fine particles 1–2 nm in size were observed for natural aging up to 70 days, but their crystal structure was stated to be unknown. Recently, S. Ramachandran et al. (submitted) employing TEM, HRTEM and

H. Conrad (✉) · S. Ramachandran · K. Jung · J. Narayan
Materials Science and Engineering Department, North Carolina State University, Raleigh, NC 27695-7907, USA
e-mail: hans_conrad@ncsu.edu

$$Al_{ss} \rightarrow \begin{Bmatrix}\text{Clusters of Si atoms}\\ \text{Clusters of Mg atoms}\end{Bmatrix} \rightarrow \begin{Bmatrix}\text{Dissolution}\\ \text{of Mg clusters}\end{Bmatrix} \rightarrow \begin{Bmatrix}\text{Formation of}\\ \text{Mg/Si co-clusters}\end{Bmatrix} \rightarrow \begin{Bmatrix}\text{Small precipitates of}\\ \text{unknown structure}\end{Bmatrix} \rightarrow \begin{Bmatrix}\beta''\\ \text{precipitates}\end{Bmatrix} \rightarrow \begin{Bmatrix}\beta'' \text{ and } B'\\ \text{precipitates}\end{Bmatrix} \rightarrow \begin{Bmatrix}\beta\, Mg_2Si\\ \text{precipitates}\end{Bmatrix}$$

Fig. 1 Precipitation sequence in the Al–Mg–Si alloy AA6061 according to Edwards et al. [4]

selected area electron diffraction (SAED), determined that the precipitates in the present Al–Mg–Si alloy AA6022 *processed without electric field and naturally aged for 2–3 years* were spherical in shape with sizes ranging from 1 nm to 40 nm in diameter (with average 4.9 nm) and had a crystal structure corresponding to the C-centered monoclinic β'' phase reported by Anderson et al. [16].

Experimental

The starting material was 1 mm thick AA6022 sheet (originally in the T4 temper) with the following composition in wt%: 0.012 Cr, 0.055 Cu, 0.13 Fe, 0.58 Mg, 0.086 Mn, 0.006 Ni, 0.76 Si, 0.02 Ti, 0.008 V, 0.011 Zn, <0.001 Zr, 0.92 Mg_2 Si and 0.40 Excess Si. ASTM standard tensile specimens with 1.2 cm wide × 5.1 cm long gage section were machined from the sheet with the tensile axis in the rolling direction. The specimens were solution heat treated (SHT) in air for 10 min at 525 ± 1.5 °C without and with a nominal dc electric field E=5 kV/cm and quenched in still water at R.T. One set of the solution heat treated specimens was then without further treatment naturally aged for specified times, while a second set was first given immediately following the quench an initial natural aging (INA) treatment of 15 min with an applied field E=5 kV/cm prior to the subsequent natural aging without a field. The electrical resistivity ρ and tensile properties following subsequent natural aging are presented in Table 3. The electrical arrangement for applying the electric field and the methods employed in the resistivity and tensile tests are presented in Refs. [1, 2]. TEM, HRTEM and SAED studies similar to those which had been performed on the specimen processed entirely without a field (S. Ramachandran et al. submitted) were carried out in the present tests on the specimen processed with the field. Details regarding the procedures in specimen preparation, TEM and HRTEM observations and the SAED analysis are given in S. Ramachandran et al. (submitted). Briefly, the TEM and HRTEM observations were performed with a JOEL JEM-2010F microscope operating at 200 kV with 0.1 nm resolution. SAED patterns were taken of: (a) the Al matrix, (b) typical small (2–40 nm) precipitates plus the Al matrix and (c) occasional large (200–500 nm) particles. The electron beam size included 10–15 of the small particles, but only a single large particle. Using the diffraction rings of the Al matrix as a standard, the lattice plane d-spacings of the precipitates and the large particles were calculated from the radii of the corresponding diffraction rings.

Table 1 Precipitation sequence and characteristics of the precipitates (ppt) in 6×××-series alloys [4–16]. Crystal lattice dimensions are in nm

Ppt. sequence	Chemistry of Ppt.	Geometry of Ppt.	Crystal Structure of Ppt.
(1) Clusters Si and clusters Mg	–	Unresolved	Vacancies included in clusters
(2) Dissolution of Mg clusters	–	Unresolved	Vacancies are involved
(3) Mg/Si clusters	Mg:Si≤1	Unresolved	GP-I Zones along <100>Al
(4) Small Ppts.	Mg:Si≤1	1–2 nm Dotty contrast, unresolved shape (spherical)	GP-II Zones, fully coherent with strain contrast
(5) β''	Mg:Si≈1	Needles along <100>Al 4–60 nm dia × 15–2000 nm long	C, centered monoclinic: a=1.53, b = 0.405, c = 0.674, $\emptyset = 105°$; Monoclinic: a = c = 0.616, b = 0.71, $\emptyset = 82°$; a = 0.30, b = 0.33, c = 0.40, $\emptyset = 71°$
(6) β'	Mg:Si≤2	Rods/Lath along <100>Al	Hexagonal: a = 0.705, c = 0.405; a = 0.407, c = 0.405
(6) Q' (B')	Al–Mg–Si–Cu 4:6:6:1 4:8:7:2 (atom ratios)	Lath	Hexagonal: a=1.04, c = 0.405; Base-Centered Orthorhombic: a = 1.8, b = 1.04, c = 0.405
(7) Q	Al–Mg–Si–Cu 4:6:6:1 4:8:7:2 (atom ratios)	Lath	Hexagonal: a = 1.04, c = 0.405
(7) β	Mg:Si = 2	Plates	CaF_2 FCC Cubic: a = 0.639

Table 2 Characteristics of the precipitates which occur during natural aging of Al–Mg–Si alloys

Composition (wt%)	t_{NA}	Method	Characteristics	Refs.
(a) 1.2 Mg_2Si (b) 1.2 Mg_2Si, 0.24 Cu	88 days	TEM	No detectable precipitation in (a) or (b).	[5]
(a) 0.58 Mg, 1.28 Si, 0.07 Cu (b) 0.55 Mg, 1.26 Si, 0.91 Cu (AA6022)	30 days	TEM DSC	Exothermic heat flow in (a) and (b). No evidence of clusters or GP zones in (a) or (b).	[6]
(a) 0.64 Mg, 1.23 Si, 0.03 Cu (b) 0.61 Mg, 1.22 Si, 0.39 Cu	7 days	TEM SAED	No indication of precipitation in (a). Dotty contrast of fine particles (~2 nm) in (b): spherical GP zones.	[7]
(a) 0.70 Mg, 0.33 Si (b) 0.65 Mg, 0.70 Si	70 days	HRTEM SADP 1DAP 3DAP	No indication of precipitate particles in (a) or (b) naturally aged. However, dark contrast rings from fine particles (~2 nm) were observed for aging 16 h at 70 °C: spherical GP zones. Mg/Si ratio in GP zone in (a) is 2:1, that in (b) is 1:1.	[8]
1.6 Mg_2Si	42 days	HRTEM	Fine particle (~1 nm) contrasts with square lattice having 0.405 nm spacing	[9]
0.43 Mg, 1.2 Si, 0.15 Cu (AA6016)	10 h–14 days	HRTEM	Strong exothermic peak at ~100 °C corresponding to formation of GPI clusters, which almost disappear after natural aging for 2 months	[10]
		DSC	Bright spots in HRTEM indicating clusters 1–2 nm in dia. after 10 h. Their size did not increase with longer natural aging time. It was not possible to define the interface as a specific plane	

Notes: t_{NA} = natural aging time; TEM = normal transmission electron microscopy; HRTEM = high resolution transmission electron microscopy, SAED = selected area electron diffraction; SADP = selected area diffraction pattern; DSC = differential scanning calorimetry, 1DAP = one dimensional atom probe; 3DAP = three dimensional atom probe

The *d*-spacings were then compared with those of planes in the crystal structures listed in Table 1 and those for Mg_2Si in the JCPDS X-ray data base [17]. For purposes of comparison and completeness, results obtained on specimens processed without field (S. Ramachandran et al. submitted) are included here along with those processed with the field. (Table 4)

Results

Figure 2 presents a TEM micrograph of the precipitates in the specimen which had been processed with an electric field applied during both SHT and INA and then naturally-aged for ~3 years. Included are SAED patterns taken of the Al matrix and of a group (10–15) of the small precipitate particles within the matrix. Enlarged views of the small precipitates are presented in the HRTEM micrographs in Fig. 3. The precipitates in Figs. 2 and 3 are approximately circular in shape, and in Fig. 3 appear to have a crystalline character. In both of these aspects they are similar to those in the specimen processed without an electric field (S. Ramachandran et al. submitted). However, they tended to be larger in size and spaced further apart than those without a field, and as will be shown below, they had a different crystal structure.

Table 3 Resistivity ρ and tensile properties of naturally aged 6022 specimens solution heat treated (SHT) 10 min at 525 °C without and with an electric field and initially aged (INA) for 15 min without and with an electric field

t_{NA}	E(kV/cm)		ρ	YS	TS	%EI
	SHT	INA	(10^{-8} Ω m)	(MPa)	(MPa)	
1 week	0	0	3.723	122	250	27
	5	0	3.845	125	255	30
	5	5	3.906	136	260	30
3 years	0	0	3.831	–	–	–
	5	0	3.871	–	–	–
	5	5	3.876	–	–	–

A comparison of the precipitate size (diameter d_p) distribution in the specimen processed with the field compared to without is given in Fig. 4. It is seen that the range in diameters (2–40 nm) is nearly the same, but there exist more particles with sizes greater than 2–3 nm for the specimen processed with an electric field. The average precipitate size for specimens processed without a field is 4.9 nm (S. Ramachandran et al. submitted), while that processed with the field is 7.9 nm. The average area fraction of the precipitates in the HRTEM micrographs such as Fig. 3 is 0.14, while that for the specimen processed without a field is 0.12. These fractions are much larger than the volume fractions expected for the amount of Mg_2Si and excess

Table 4 Matching of lattice plane *d*-spacings determined from the SAED patterns of the small circular-shaped precipitates in the specimens processed without and with an electric field with those of specific crystal structures in the literature

Processed without field (S. Ramachandran et al. submitted)			Processed with field		
Ring radius (nm)	Calc. *d*-spacing ppt. (nm)	*d*-spacing crystal plane (nm)	Ring radius (nm)	Calc. *d*-spacing ppt. (nm)	*d*-spacing crystal plane (nm)
3.5	4.343	4.10(010)β''[a]	4.5	3.103	?[b]
6	2.533	2.48(012)β''	5	3.036	?
7	2.171	2.02(020)β''	6	2.53	?
8	1.900	1.93(021)β''	10	1.518	?
10	1.520	0.40(110)β''	13	1.118	?
11.5	1.322	1.30(111)β''			
13	1.169	1.19(120)β''			
14.5	1.048	1.00(130)β''			
17.3	0.879	0.89(007)β''			
19	0.800	0.70(211)β''			
24.5	0.620	0.67(221)β''			

[a] Crystal structure of β'' is C-centered monoclinic with $a = 1.53$ nm, $b = 0.405$ nm, $c = 0.674$ nm and $\varphi = 105°$ [16]; [b] Crystal structure of precipitate in unknown

Si present in the alloy. This can be attributed to the fact that the HRTEM micrographs were generally taken of regions where the largest number of precipitates existed.

The lattice plane *d*-spacings calculated from the radii of the diffraction rings in the SAED patterns of the small precipitates are presented in Table 4 for the specimens processed without and with the electric field. A good match occurs between the calculated *d*-spacings and various planes in the C-centered monoclinic β'' phase (GP-II zone) [16] for the specimen processed without the field. In contrast, no clear matching occurred with β'' or with any of the other crystal structures listed in Table 1 for the specimen processed with the field. *Hence, the field has affected the crystal structure of the precipitates as well as their size, spacing and size distribution.*

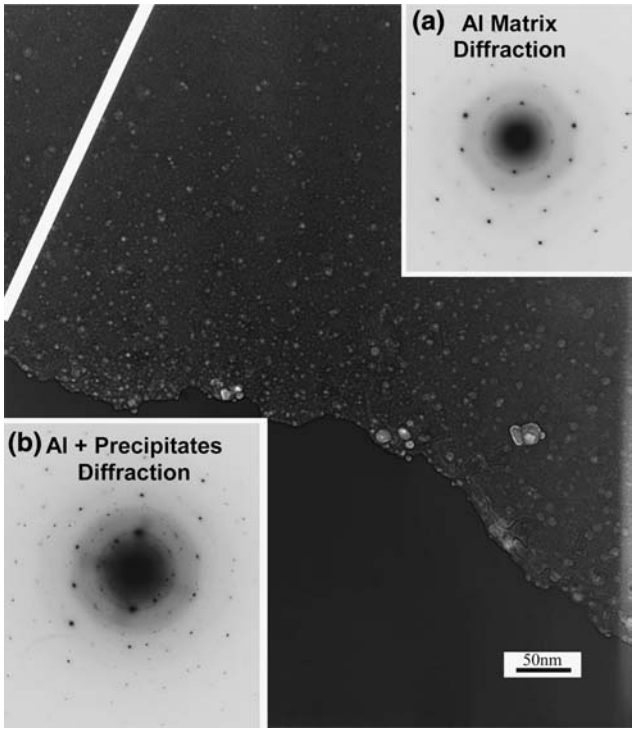

Fig. 2 TEM micrograph of the precipitates in the specimen processed with electric field. Included are SAED patterns of: (**a**) Al matrix and (**b**) the small precipitates plus Al matrix

Besides the fine circular-shaped precipitates, there existed occasional large rectangular-shaped particles (~200 × 500 nm^2); see Fig. 5. The lattice *d*-spacings of these particles calculated from the diffraction rings are given in Table 5. There is a good match of the *d*-spacings of the particle in the specimen processed with the field with those of the metastable Mg_2Si-II phase listed in the JCPDF XRD database [17], suggesting it may be undissolved Mg_2Si. No clear matching with any phase in Table 1 or in the JCPDF database for Mg_2Si was found for the large particles in the specimen processed without field.

Discussion

The TEM and HRTEM micrographs and the SAED analyses indicate that the application of an electric field during SHT and INA not only influenced the size, spacing, size distribution and volume fraction of the precipitates which occurred with subsequent natural aging for 2–3 years, but also affected their crystal structure. The observed increase in volume fraction is in keeping with the increase in solubility corresponding to the decrease in the Gibbs free energy of solution ΔC_8 produced by the field applied during SHT [1, 2]. Since an electric field applied only during SHT had no

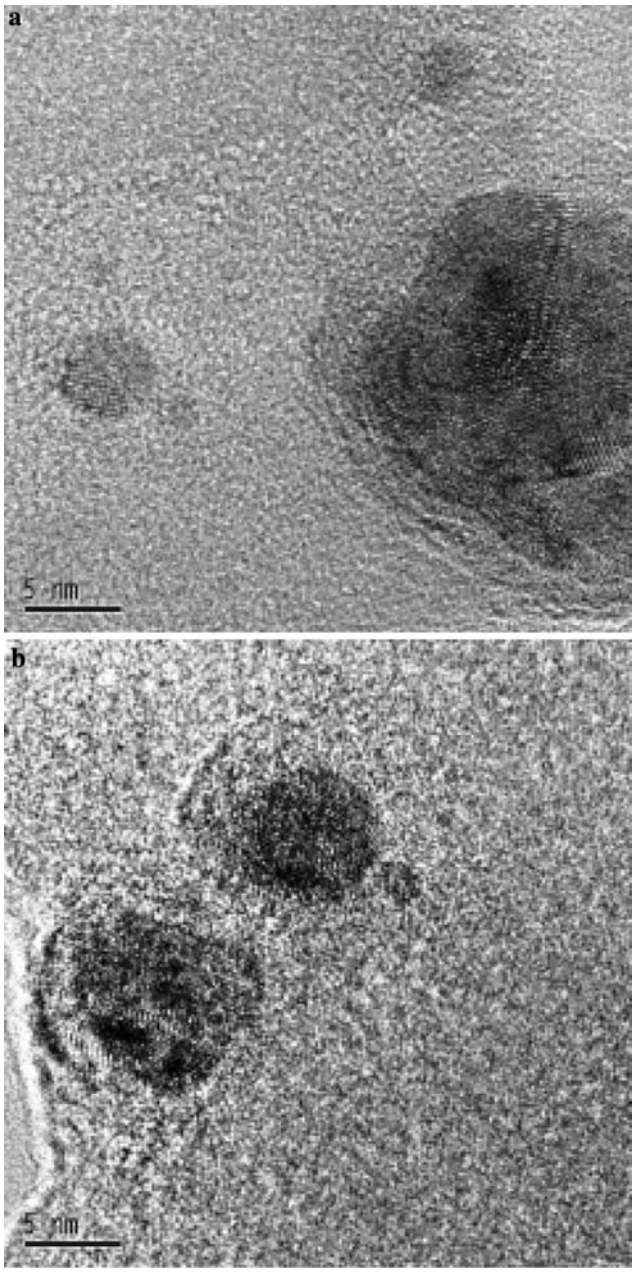

Fig. 3 HRTEM view of the precipitates in the specimen processed with electric field: (**a**) in the grain interior and (**b**) near a grain boundary

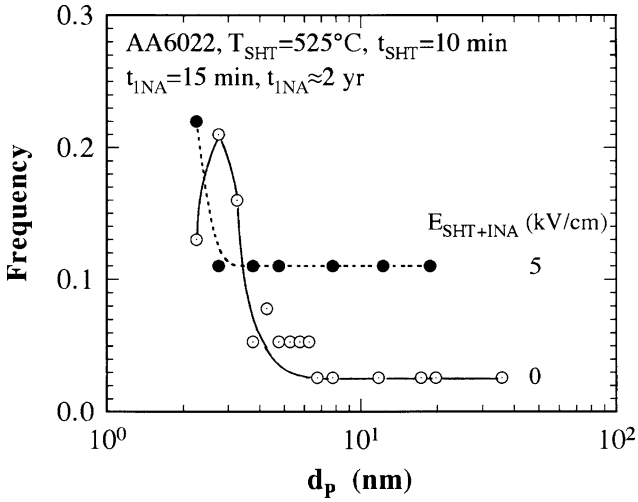

Fig. 4 Comparison of the size distribution of the precipitates in the specimen processed with electric field with that of the precipitates in the specimen processed without field. Data without a field from S. Ramachandran et al. (submitted)

$$\sigma_{\mathrm{ppt}} = \frac{M(F*)^{3/2} f^{1/2}}{b\left(2\sqrt{3}\pi\right)^{1/2} \Gamma^{1/2} r^*} \tag{1}$$

where M is the Taylor orientation factor, F^* is the maximum interaction force between dislocations and an average-size precipitate of radius r^*, f the volume fraction of precipitates and Γ the dislocation line tension. The increase in yield stress (in the T4 temper) which occurred here with application of the electric field during SHT and INA would then be due to an increase in the ratio $(F*)^{3/2} f^{1/2}/r*$. Assuming that the actual volume fractions f are proportional to those determined from the HRTEM micrographs and taking the magnitudes of d_{p}(avg) and f(avg), the ratio $f^{1/2}/r^*$=0.095 nm^{-1} with the field compared to 0.141 nm^{-1} without. In view of the smaller value of this ratio, the observed increase in yield stress with the field treatment thus appears to be due to an increase in F^*, which in turn could result from both the larger size of the precipitates and their different crystal structure.

effect on the natural aging kinetics measured by resistivity (K. Jung and H. Conrad submitted; H. Conrad and K. Jung submitted), the increase in the size of the precipitates observed here with the field could result from a reduction in the number of nuclei, rather than from an increase in their growth rate.

Esmaeili et al. [18] have proposed that the yield stress component due to the clusters or precipitates which occur during natural aging in Al–Mg–Si alloys is given by

The physical mechanism(s) by which an electric field can affect the solubility during SHT and the subsequent size, size distribution, spacing and crystal structure of the precipitates which occur during natural aging is not clear. The influence of a field during SHT could be either by directly affecting the energy of charged vacancy-solute atom complexes within the interior of the specimens, or indirectly thorugh the interaction of such charged complexes with the charged surface. Likewise, any influence of an electric field applied during INA could also result from the above-mentioned direct or indirect effects. Further

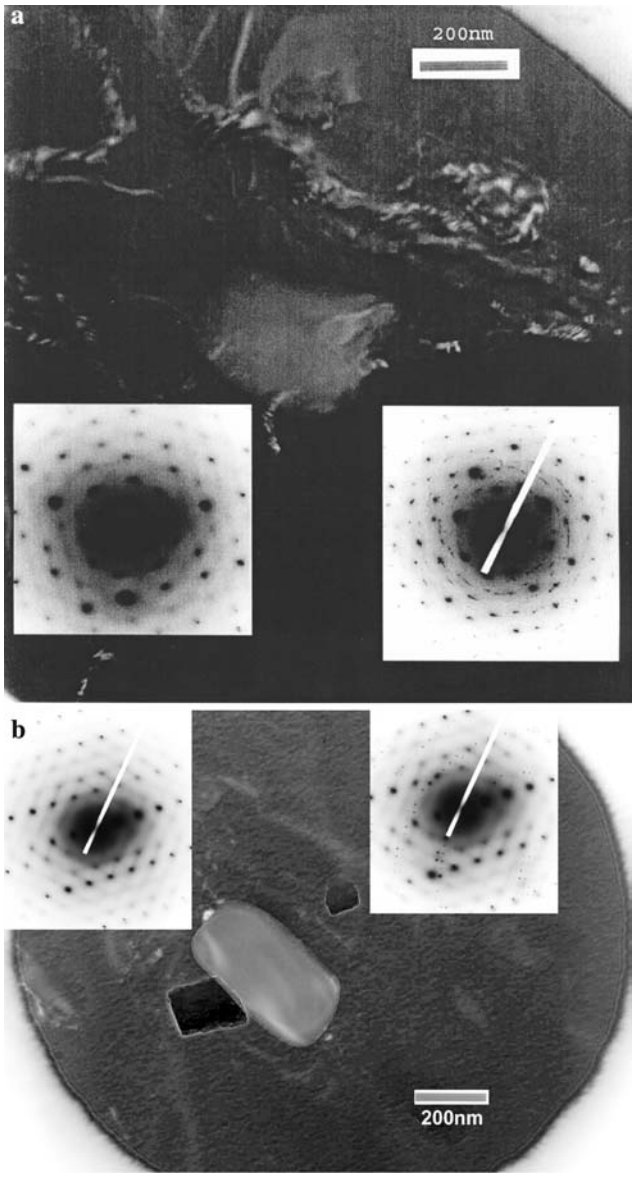

Fig. 5 TEM micrograph of the occasional large rectangular-shaped particles: (**a**) specimen processed with electric field and (**b**) processed without field

work is needed to resolve which of these effects of the field may be responsible for the observed behavior.

Summary and conclusions

TEM, HRTEM and SAED were employed to determine the influence of an electric field applied during solution heat treatment (SHT) and during a short initial natural aging (INA) treatment on the nature of the precipitates which subsequently occurred with long-time (2–3 years) natural aging of AA6022. The following are the results obtained and the conclusions derived therefrom.

1. The precipitates with the field treatments were approximately spherical in shape with an average diameter of 7.9 nm; those without the field were of similar shape but had an average diameter of 4.9 nm and were more closely spaced.
2. The range in precipitate size (2–40 μm) with the field treatments was the same as that without, but there occurred more particles with a size >3 nm in the specimen treated with the field.
3. The calculated lattice *d*-spacings of the crystal structure of the precipitates in the specimen processed with electric field did not match any of the crystal structures in the literature for precipitates in Al–Mg–Si alloys. In contrast, the calculated lattice *d*-spacings of the precipitates in specimens processed without a field matched those of the C-centered monoclinic β'' (GP-II) phase.
4. The lattice *d*-spacings of occasional large rectangular-shaped particles (200–500 nm) in the specimen processed with electric field matched those of the metastable hexagonal Mg_2Si phase. No clear matching for similar particles in the specimen processed without a field was found.

Table 5 Matching of lattice plane d-spacings determined from the SAED patterns of the large rectangular-shaped precipitates in specimens processed without and with an electric field with those of specific crystal structures in the literature

Processed without field			Processed with field		
Ring radius (nm)	Calc. *d*-spacing ppt. (nm)	*d*-spacing crystal plane (nm)	Ring radius (nm)	Calc. *d*-spacing ppt. (nm)	*d*-spacing crystal plane (nm)
5.0	3.273	?[a]	6.0	2.72	2.71(311) Hexβ''[b]
5.8	2.822	?[a]	6.6	2.48	2.48(401) Hexβ''
7.8	2.090	?[a]	7.0	2.34	2.34(410) Hexβ''
9.7	1.687	?[a]	8.1	2.02	2.03(420) Hexβ''
15	1.091	?[a]			1.48(423) Hexβ''
16.5	0.990	?[a]			1.60(611) Hexβ''

[a] Crystal structure is not known; [b] Lattice *d*-spacings for metastable hexagonal Mg_2Si-II β'' phase taken from JCPD XRD data base [17]

5. The increase in yield stress, which occurred with the electric field treatments appears to result from an increase in the interaction force between the precipitates and dislocations.

Acknowledgements This research was funded by the U.S. Army Research Laboratories and the U.S. Army Research Office under Award DAA1902-1-0315 with Dr. William Mullins as contract monitor. The authors also wish to thank Dr. R. Ramage, Alcoa Technical Center, for providing the AA6022 material and Dr. D. Lloyd, Novelis Global Technology Center, for the chemical analysis and helpful discussions. We also wish to thank Ms. R. O'Connell for typing the manuscript.

References

1. Jung K, Conrad H (2004) J Mater Sci 39:6481
2. Conrad H, Jung K (2004) Z f Matallkde 95:352
3. Conrad H, Jung K, Unpublished research North Carolina State University (2004)
4. Edwards GA, Stiller K, Dunlop GL, Couper MJ (1998) Acta Mater 46:3893
5. Pashley DW, Rhodes JW, Sendorek A (1966) J Inst Mat 94:41
6. Miao E, Laughlin DE (2000) Metall Mater Trans A 31A:361
7. Murayama M, Hono K, Miao WF, Laughlin DE (2001) Metall Mater Trans A 32A:239
8. Murayama M, Hono K (1999) Acta Mater 47:1537
9. Matsuda K, Kawabata T, Uetami Y, Sato T, Kamio A, Susumu K (2000) Mater Sci Forum 331–337:989
10. Zhuang L, Janse JE, De Smer P, Chen JH, Zandberger HW, in Aluminum 2001: Proc. TMS 2001 Aluminum, Automotive and Joining Sessions, TMS Warrendale, PA (2001), p 77
11. Matsuda K, Uetani Y, Sato T, Ikeno S (2001) Matell Mater Trans A 32A:1293
12. Matsuda K, Karabata T, Uetani Y, Sato T, Ikena S (2002) Scripta Mater 47:467
13. Perovic A, Perovic DD, Weatherly GC, Lloyd DJ (1999) Scripta Mater 41:703
14. Weatherly GC, Perovic A, Mukhopadhyay NK, Lloyd DJ, Perovic DD (2001) Metall Mater Trans A 32A:21
15. Esmaeili S, Wang X, Lloyd DJ, Poole WJ (2003) Metall Mater Trans A 34A:751
16. Anderson SJ, Sandberger HW, Jansen J, Traeholt C, Tundel U, Reiso O (1998) Acta Mater 46:3238
17. JCPDS-ICDD data base: PDF-2 Data Base (Sets 1–39) PDF-2 39 6A June 89 (1989)
18. Emaeili S, Lloyd DJ, Poole WJ (2003) Acta Mater 51:2243